Global increase of p16INK4a in APC-deficient mouse liver drives clonal growth of p16INK4a negative tumors

Ueberham, E., Glockner, P., Gohler, C., Straub, B.K., Teupser, D., Schonig, K., Braeuning, A., Hohn, A.K., Jerchow, B., Birchmeier, W., Gaunitz, F., Arendt, T., Sansom, O., Gebhardt, R., Ueberham, U.

Molecular Cancer Research
2015 FEB ; 13(2): 239-249
Published first September 30, 2014
doi: 10.1158/1541-7786.MCR-14-0278-T

Global Increase of p16^{INK4a} in APC-deficient Mouse Liver Drives Clonal Growth of p16^{INK4a} Negative Tumors

Elke Ueberham[1,11], Pia Glöckner[2], Claudia Göhler[1], Beate K. Straub[3], Daniel Teupser[4,12], Kai Schönig[5], Albert Braeuning[6], Anne Kathrin Höhn[7], Boris Jerchow[8], Walter Birchmeier[8], Frank Gaunitz[9], Thomas Arendt[2], Owen Sansom[10], Rolf Gebhardt[1,*], Uwe Ueberham[2,*,#]

[1]Faculty of Medicine, University of Leipzig, Institute of Biochemistry, Johannisallee 30, Leipzig, 04103, Germany
[2]Department for Molecular and Cellular Mechanisms of Neurodegeneration, University of Leipzig, Paul Flechsig Institute of Brain Research, Jahnallee 59, Leipzig, 04109, Germany
[3]Institute of Pathology, University Clinic, University Heidelberg, Im Neuenheimer Feld 224, Heidelberg, 69120, Germany
[4]Institute of Laboratory Medicine, Clinical Chemistry and Molecular Diagnostics, University of Leipzig, Liebigstr. 27, Leipzig, 04103, Germany
[5]Central Institute of Mental Health, Department of Molecular Biology, University of Heidelberg, J5, Mannheim, 68159, Germany
[6]Department of Toxicology, Institute of Experimental and Clinical Pharmacology and Toxicology, Wilhelmstr. 56, Tübingen 72074, Germany
[7]Institute of Pathology, University of Leipzig, Liebigstr. 24, 04103 Germany
[8]Max-Delbrueck-Center for Molecular Medicine, Robert-Roessle-Str. 10, Berlin-Buch, 13125, Germany
[9]Department of Neurosurgery, University of Leipzig, Liebigstr.20, Leipzig, 04103, Germany
[10]The Beatson Institute for Cancer Research, Garscube Estate, Switchback Road Glasgow, G61 1BD, United Kingdom
[11]Fraunhofer Institute for Cell Therapy and Immunology, Perlickstr. 1, 04103 Leipzig, Germany
[12]Institute of Laboratory Medicine, Ludwig-Maximilians-University Munich, Marchioninistrasse 15, 81377 Munich, Germany
[*]indicates shared senior authorship

Disclosure Statement:

The authors disclose no potential conflicts of interest.

[#]Corresponding author:
Uwe Ueberham, Ph.D.
Paul Flechsig Institute of Brain Research
Department for Molecular and Cellular Mechanisms of Neurodegeneration
Jahnallee 59, D-04109 Leipzig
Germany
Tel.:-49-(341)-9725737
Fax:-49-(341)-9725729
e-mail: Uwe.Ueberham@medizin.uni-leipzig.de

Keywords: $p16^{INK4a}$, adenomatous polyposis coli, APC, liver tumor, β-catenin, mouse model, Apc^{580S}, CTNNB1

Running title: $p16^{INK4a}$ and APC in liver tumors

Grant Support:

Parts of this work were financially supported by the European Union (grant CancerSys 223188), by the BMBF (01EW0907) in the frame of ERA-Net Neuron and the AFI-Project 984000-150 as well as the DFG (STR 1160/1-1)

Abstract

Reduction of β-catenin (CTNNB1) destroying complex components, e.g. adenomatous polyposis coli (APC), induces β-catenin signaling and subsequently triggers activation of genes involved in proliferation and tumorigenesis. Though diminished expression of APC has organ specific and threshold dependent influence on the development of liver tumors in mice, the molecular basis is poorly understood. Therefore, a detailed investigation was conducted to determine the underlying mechanism in the development of liver tumors under reduced APC levels. Mouse liver at different developmental stages was analyzed in terms of β-catenin target genes including *Cyp2e1*, *Glul* and *Ihh* using real-time RT-PCR, reporter gene assays and immunohistological methods with consideration of liver zonation. Data from human livers with mutations in *APC* derived from FAP patients were also included. Hepatocyte senescence was investigated by determining $p16^{INK4a}$ expression level, presence of senescence-associated β-galactosidase (SA-β-Gal) activity and assessing ploidy. A β-catenin activation of hepatocytes does not always result in β-catenin positivity but unexpectedly also in mixed and β-catenin negative tumors. In summary, a senescence inducing program was found in hepatocytes with increased β-catenin levels and a positive selection of hepatocytes lacking $p16^{INK4a}$, by epigenetic silencing, drives the development of liver tumors in mice with reduced APC expression (Apc^{580S} mice). The lack of $p16^{INK4a}$ was also detected in liver tumors of mice with triggers other than APC reduction.

Implications

Epigenetic silencing of $p16^{Ink4a}$ in selected liver cells bypassing senescence is a general principle for development of liver tumors with β-catenin involvement in mice independent of the initial stimulus.

Introduction

Genesis of hepatocellular carcinoma (HCC) is not fully understood, though several carcinogenic pathways involved in this process were identified (1) among them the Wnt/β-catenin pathway. Activated β-catenin (CTNNB1) signaling contributes to approximately 30% of HCCs (2, 3) and is characterised by nuclear and/or cytoplasmic staining of β-catenin (4) which contrasts to cell membranous staining of unaffected liver. Consequently, Wnt/β-catenin target genes, i.e. *glutamine synthetase* (*Glul*) (5), are upregulated in β-catenin positive HCCs. Induction of β-catenin signaling in HCCs is caused by gain of function mutations in *β–catenin* (6) or mutations in genes coding for components of the β-catenin destruction complex, i.e. AXIN1 (7) or AXIN2 (8). Though, mutations of adenomatous polyposis coli (*APC*) gene, a further constituent of β-catenin destruction complex, are rarely detected in primary liver cancer (9), methylation of *APC* promoter seems significant in HCC suggesting functional importance of altered APC levels (10). In contrast, other malignancies of gastrointestinal cancer, i.e. colon and rectal cancers, are strongly predisposed to *APC* germline mutations, as found in familial adenomatous polyposis (FAP, (11)). Recently, context specific responsiveness for Wnt/β-catenin signaling has been suggested necessary to develop cancer following APC reduction (12). Buchert reported development of HCCs in livers of aged homozygous Apc^{580S} mice expressing reduced APC levels (13). Unexpectedly, HCCs of this model display a downregulation of the Wnt-target gene (14) *Axin2*, suggesting its reduction in tumors might have promoted HCC formation at the long latencies observed in these mice.

However, the tumors lacked hypermethylation of *Axin2* promoter (12). Moreover, additional events causing tumorigenesis in this model were still unclear as mutations in oncogenes, i.e. *Hras*, were not observed. Therefore, the mechanism of how APC reduction promotes HCC development remains ambiguous and important to elucidate.

Here we investigate potential mechanisms supporting development of HCCs in livers with reduced APC levels. To this end, we utilise *Apc*^{580S} mice (13) exhibiting elevated β-catenin levels and investigate deregulation of Wnt signaling during all stages of HCC development. By comparing expression pattern in isolated hepatocytes and liver tissue of transgenic mice with different levels of β-catenin, which were generated with the help of the tet-inducible expression system, we inferred a concerted action of a senescence inducing program in hepatocytes with increased β-catenin levels and a positive selection for hepatocytes with loss of cell-cycle inhibitor p16^{INK4a} (CDKN2A) (15) as driver for the development of liver tumors in *Apc*^{580S} mice.

Materials and Methods

Mice

An overview of transgenic mice is presented in Supplementary Table S1. *Apc*^{580S} (13) mice, termed *Apc*^{homo}, carry a homozygous floxed exon 14 *Apc* allele. *Ctnnb1*$^{flox/flox}$ (16) mice, termed *Ctnnb1*^{homo}, were purchased from Jackson Laboratories. Three knock-out (KO) mice, *Apc*^{KO}, *Ctnnb1*^{KO} and *Apc*^{KO}/*Ctnnb1*^{KO} were obtained by interbreeding of floxed mice with liver specific inducible *Cre* mice (17) carrying inducible *P*$_{tet}$*Cre-recombinase* (*LC-1*) and tetracycline controlled transactivator (*TA*^{LAP2}) transgenes (18). Homozygous *P*$_{tet}$*Cre-Apc*^{homo} mice were bred with homozygous *TA*^{LAP2}*-Apc*^{homo} mice to obtain *P*$_{tet}$*Cre-TA*^{LAP2}*-Apc*^{homo} which after induction by doxycycline withdrawal result in *Apc*^{KO} (for breeding schema see Supplementary Fig.S1). Accordingly, interbreeding was performed with *Ctnnb1*^{homo} and combined *Apc*^{homo}/*Ctnnb1*^{homo} mice leading to *Ctnnb1*^{KO} or *Apc*^{KO}/*Ctnnb1*^{KO} mice (Supplementary Tab.S1). *Conductin*$^{+/lacZ}$ mice in which the reporter enzyme β-galactosidase is controlled by endogenous *Conductin* (*Axin2*) promoter were interbred with *Apc*^{homo} mice and other lines specified above to obtain *Apc*^{hetero}/*Conductin*$^{+/lacZ}$, *Apc*^{homo}/*Conductin*$^{+/lacZ}$ and

Apc^{KO}/*Conductin*$^{+/lacZ}$ mice, respectively. Mice used in proliferation tests received a unique BrdU injection (i.p.,10mM, 0.01ml/g body weight) two hours before killing.

Human tissue samples

Human specimens were provided by the Tissue Bank of the National Center for Tumour Diseases (Heidelberg, Germany, ethics proposal 206/2005, University Heidelberg). 14 formalin-fixed, paraffin-embedded liver specimens mostly taken from partial hepatectomies for liver metastases of colorectal cancer excised far from the metastases were investigated. Seven patients had clinically known FAP.

Histochemistry and immunohistochemistry

Immunohistochemistry was performed as described (19, 20). Briefly, 5-µm paraffin sections were dewaxed with xylol and hydrated through downward alcohol series. Antigen retrieval was assessed by microwaving in citrate buffer (pH 6.0). Slides were equilibrated in Tris-buffered saline (pH 7.4), quenched with H_2O_2, blocked with biotin/avidin, and goat serum and Blocking Reagent (VECTOR^{TM} M.O.M. Immunodetection Kit) for mouse antibodies respectively, and incubated with primary antibodies (listed in Supplementary Tab.S2) overnight at 4°C. Corresponding biotinylated secondary antibodies were coated for 1 hour at room temperature. After washing slides were incubated with extravidin-POD conjugate and washed three times before staining with 3,3'-diaminobenzidine-tetrahydrochloride (DAB). POD oxidises DAB producing a brown precipitate. For p16^{INK4a} immunohistochemistry human liver sections were stained automatically by a Ventana Nexes autostainer (Ventana, Tucson, USA) using CINtec® p16 (E6H4) immunohistochemistry.

Senescence associated β-galactosidase (SA-β-Gal)

Frozen liver samples were cut and mounted on Superfrost plus slides (Menzel, Braunschweig, Germany). Slides were dried 1 hour at room temperature and fixed with 0.5% glutaraldehyde in PBS 5 min at room temperature. After washing in PBS slides were incubated in 40 mM Na_2HPO_4, 40 mM citrate pH 6.0, stained overnight at 37°C with 1 mg/ml 5-bromo-4-chloro-

3-indolyl-beta-D-galactoside (X-Gal) in 40 mM citric acid, sodium phosphate, pH 6.0, 5 mM potassium ferrocyanide, 5 mM potassium ferricyanide, 150 mM NaCl and 2 mM $MgCl_2$.and counterstained with hematoxylin.

Reporter enzyme

Sections were fixed in 2% paraformaldehyde and 0.2% glutaraldehyde in PBS pH 7.4 for 30 min at room temperature, washed three times for 15 min with 2 mM $MgCl_2$, 0.01% Nonidet P-40 in PBS and stained with 1 mg/ml X-Gal, 5 mM $K_3Fe(CN)_6$, 5 mM $K_4Fe(CN)_6$ for 36–40 h at 37 °C in the dark. Slides were counterstained with nuclear fast red.

Isolation of hepatocytes, cell culture and transfection

Primary hepatocytes were isolated and cultivated as described (20) by collagenase perfusion (21). Pericentral and periportal hepatocytes were isolated by a modified digitonin/collagenase perfusion technique (22, 23) and transfected with TOP-Gau reporter plasmids (24) using Effectene (Qiagen). *Apc* silencing *in vitro* was achieved by transfection with *Apc* siRNA (APCMSS202103, APCMSS202104, APCMSS202105, Invitrogen, 4nM) using Interferin (PeqLab).

Gaussia luciferase assay

Gaussia luciferase activity was measured in 10 µl supernatant of transfected hepatocytes with 50 µl assay reagent on Orion-II microplate luminometer (Titertek-Berthold).

RNA isolation and quantitative real-time reverse transcription PCR (qRT-PCR)

Total RNA was isolated using PeqGOLD RNA Pure isolation system (Peqlab). RNA quality was assessed by gel electrophoresis and purity was estimated using the A260/A280 ratio. Concentration was adjusted to 0.5 mg/ml. qRT-PCR was performed as described (20) using primers listed in Supplementary Table S3. RNA load was normalised with the housekeeping gene *cyclophilin* (*Ppia*). Standard curves of serial dilutions from total RNA were used for transforming ct-values to concentration values depicted as arbitrary units.

Methylation-specific PCR

DNA from tumor and surrounding liver tissue was isolated using NucleoSpin tissue kit (Macherey&Nagel). DNA methylation was tested with the bisulfite conversion method using the EZ DNA-Methylation-Gold kit (Zymo Research) and $p16^{Ink4a}$ promoter-specific primers (25) Supplementary Table S3).

Clinical Chemistry

Alanine aminotransferase (ALAT) and glutamate dehydrogenase (GLDH) were measured on an automated clinical chemistry analyzer (Modular PPE, Roche).

Flow cytometry

Hepatocytes were counted and 200,000 cells were resuspended in 100 µl wash buffer (PBS, 5% FCS). After washing, 500 µl prechilled ethanol (-20°C) was added slowly with continuous mixing avoiding agglutination. Hepatocytes were kept on ice, washed twice with 1 ml PBS/5% FCS and incubated for 1 hour with RNAse A (1mg/ml PBS) at 37°C. Suspensions were brought up to 200 µl with PBS/5% FCS and 20 µl propidium iodide (1 mg/ml) was added. This hepatocyte suspension was measured on a flow cytometer (FACScan, BD Biosciences) for determining the ploidy grade.

Statistical analysis

All data are expressed as mean ± S.E.M. Statistical analysis was performed by Student's t-test or Mann-Whitney test using SigmaPlot 11 (SSP Science). The accepted level of significance was set at $p<0.05$.

Results

Activation of β–catenin initiates AXIN2 expression in selected/individual HCCs of aged Apc^{homo} mice

Using liver sections β-catenin signaling was investigated by immunohistochemistry in hepatocytes of young (8 weeks) and aged (10 months) Apc^{homo} and compared to Apc^{KO} mice representing a positive control for β-catenin activation (Figs.1A-D). This staining displayed

only few hepatocytes with activated β-catenin (nuclear expression) both in liver tissue from young Apc^{homo} mice and tissue adjacent to tumors in aged mice. Liver tumors and their prestages in aged Apc^{homo} mice exhibit, unexpectedly, a highly heterogeneous β-catenin staining in the same animal. Both β-catenin negative (Fig.1C,C') and β-catenin positive (Fig.1D,D') tumors were detected. Moreover, if tumors contained activated β-catenin they always displayed membrane-bound β-catenin providing a mixed phenotype, while an exclusively nuclear or cytoplasmic staining was never detectable.

Quantification of the universal and direct Wnt/β-catenin target gene, *Axin2* mRNA level in liver tissue extracts (Fig.1E), expectedly revealed a significant elevation in Apc^{homo} and Apc^{KO} and a decrease by trend in $Ctnnb1^{KO}$ mice (only 2 animals were investigated due to sudden early death of $Ctnnb1^{KO}$ mice) and a significant decrease in $Apc^{KO}/Ctnnb1^{KO}$ mice compared to controls (both heterozygous and wild-type mice). In contrast, *Axin2* mRNA levels in tumor extract (containing several tumors) were not significantly altered (Fig.1E). However, re-evaluation of macroscopically visible tumors and subsequent resection of individual tumors of each liver revealed different individual *Axin2* mRNA levels (Fig.1F). Thereby, in the same animal either up- or downregulation of the β-catenin responsive target *Axin2* occur in individual HCCs.To functionally validate activation of β-catenin signaling *in vitro* we transfected a TCF-reporter, which allows monitoring activity of β-catenin triggers, in isolated primary hepatocytes (Fig.1G). Hepatocytes from Apc^{homo} mice show a 5fold induction of *Gaussia* luciferase activity compared to controls, and in turn represent about one-fifth of luciferase activity obtained in Apc^{KO} mice (Fig.1G), thus supporting *Axin2* mRNA data.

In vivo we also confirmed the elevated activation of β-catenin signaling in Apc^{homo} mice utilizing the Wnt reporter mouse $Conductin^{+/lacZ}$ in which the reporter gene *β-galactosidase* is expressed in response to the endogenous *Conductin* (*Axin2*) promoter. In $Apc^{hetero}/Conductin^{+/lacZ}$ mice β-galactosidase was detected only in pericentral hepatocytes as

a weak spot-like staining within the nucleus of the first row of cells around central veins and rarely in the second row, while midzonal or periportal hepatocytes were never positively marked (Fig.1H). In Apc^{homo} mice (Fig.1J) the expression zone expanded and staining intensity increased. Here, several individual midzonal hepatocytes show β-galactosidase activity.

β-catenin target genes are heterogenously expressed in tumors and lesions

We examined expression of common β-catenin target genes, *Glul* and *Cyp2e1* (*Cytochrome P450 2E1*) (Fig.2A), representing classical pericentrally (pc) expressed proteins within livers of Apc^{homo} mice at different ages. Additionally, we inspected the pattern of typical periportally (pp) expressed proteins, carbamoyl phosphate synthetase I (CPS) and E-cadherin, which are expected to be conversely localized to pc-specific proteins (Fig.2A). Liver tissue of Apc^{homo} mice showed age-dependent up-regulation of β-catenin target genes, *Cyp2e1* and *Glul*, supporting data from Buchert and collegues (12), who investigated five-months-old mice. The cellular proportion of the pericentral expression type in the zonal expression pattern starts to increase at age 3 weeks and is nearly completed at age 8 weeks. Later on, in mice, over five months old (Fig.2A), first cancerous lesions appear. Although there was a slight increase of hepatocytes exhibiting nuclear/cytoplasmic β-catenin in aged Apc^{homo} mice, GLUL expression never spread over the whole lobulus.

The shifted zonal expression pattern of pericentral and periportal proteins in liver parenchyma of Apc^{homo} mice as a result of a continuous moderate activation of β-catenin signaling raised the question whether zonal shifting in liver parenchyma also occurs in patients with *APC*-repressing mutations. Thus we examined the zonal expression pattern of GLUL in paraffin sections of livers of FAP patients (Fig.2B). In six out of seven FAP liver samples enlargement of the GLUL positive zone was detected. In two of these six samples GLUL positive focal

nodular hyperplasia was demonstrated (Fig.2B, top right), whereas GLUL positive nodules were not present in controls.

Precancerous lesions and tumors of aged *Apc*^{homo} mice, however, feature surprising heterogeneity regarding the expression of the β-catenin target genes, *Glul* and *Cyp2e1* (Fig.3). As expected from nuclear/cytoplasmic β-catenin staining pattern and *Axin2* mRNA quantification tumors with pericentral, periportal or the mixed expression program were detected within an individual animal (Fig.3).

p16^{INK4a} expression is regulated by β-catenin and loss of p16^{INK4a} is characteristic for all tumors and precancerous lesions

The mechanism driving carcinogenesis in *Apc*^{homo} mice seems obscure, because β-catenin dependent hepatocyte proliferation is supposed not to be cell-autonomous (26) and tumors with homogenously nuclear β-catenin staining were not found in our experiments. Moreover, hyperproliferation neither of hepatocytes carrying nuclear or cytoplasmic β-catenin nor of pc-re-programmed GLUL positive hepatocytes occurs in *Apc*^{homo} mice (Supplementary Fig.S2). A pronounced proliferation in non-tumorous liver parenchyma was detected in livers of *Apc*^{KO} mice only (Supplementary Fig.S2,C) compared to coeval *Apc*^{homo} and control mice (Supplementary Fig.S2A,B). However, the hyperproliferation in *Apc*^{KO} mice is accompanied with ruin of hepatocytes by necrosis (Fig.7A,B; black arrows). However, preliminary microarray experiments comparing the mRNA expression pattern of pericentral hepatocytes from *Apc*^{homo} mice to periportal hepatocytes from *Apc*^{hetero} mice, indicate alterations of tumor suppressor levels in pericentral hepatocytes. Furthermore, tumor suppressor *p16*^{INK4a} was recently identified as a β-catenin target gene (27). Both results suggest p16^{INK4a} as a possible key regulator for tumorigenesis in *Apc*^{homo} mice. Consequently, we analyzed p16^{INK4a} immunohistochemically and detected a very high cytoplasmic amount of p16^{INK4a} in nearly all hepatocytes in aged *Apc*^{homo} mice independently of their acinar location (Supplementary

Fig.S3,S4). Livers of FAP patients were also examined concerning expression of $p16^{INK4a}$. Hereby both stainings manually performed with monoclonal antibody D7D7 used for detection of $p16^{INK4a}$ negative lesions in mice (not shown) and automatically performed with monoclononal antibody E6H4 (CINtec® p16,) (Supplementary Fig.S3) detected a pronounced incidence of $p16^{INK4a}$ in all livers samples of FAP patients compared to normal liver. Thereby a preference of $p16^{INK4a}$ expression in pericentral areas was observed in both FAP livers and controls (frames in Supplementary Fig.S3J,K and the corresponding magnifications J' and K').

Simultaneously, loss of $p16^{INK4a}$ protein in all mouse liver tumors and precancerous lesions (Fig.4A) was detected. Serial sections of liver tissue from mice at age 10 months or older showing macroscopically visible tumors corroborate the $p16^{INK4a}$ negativity of tumors and prestages independently on whether a periportal or pericentral expression program was followed (Fig.4A). Cells within the $p16^{INK4a}$ negative tumors proliferate which is shown by BrdU incorporation (Supplementary Fig.S2E,E'). In contrast tumor surrounding hepatocytes which are characterized by high $p16^{INKa}$ expression do not proliferate (Supplementary Fig.S2E').

To confirm $p16^{INK4a}$ protein deficiency as a general hallmark of HCCs in mice with abnormal β-catenin signaling, we stained liver sections harbouring tumors, which initial causative event had been identified as activating mutations in exon 3 of the CTNNB1 proto-oncogene, leading to constitutively active Wnt/β-catenin signaling, ((28), Fig.4C) and tumors, which developed after transfection of $Apc^{flox/flox}$ mice using a virally encoded *Cre-recombinase* ((29), Fig.4B). All tumors including those with different genesis were $p16^{INK4a}$ protein negative. In contrast, liver tumors of aged Apc^{homo} mice displayed no reduction of other tumor suppressors i.e. $p19^{ARF}$, $p15^{INK4b}$ or $p21^{CIP1}$ (data not shown). Higher $p16^{Ink4a}$ mRNA expression level was found in pericentral hepatocytes of Apc^{homo} mice (moderate activation of β-catenin signaling)

and hepatocytes of *Apc*^{KO} mice (highest β-catenin signaling) compared to hepatocytes of *Apc*^{hetero} mice (low β-catenin signaling) (Fig.5B).

Cause of p16^{INK4a} deficiency in tumors of *Apc*^{homo} mice

The downregulation of p16^{INK4a} protein in tumors of *Apc*^{homo} mice matches data on kidney (30), showing that only bypassing senescence caused by p21^{CIP1} triggers renal tumors in *Apc*^{homo} mice. In liver *p16*^{Ink4a} silencing seems to meet this function.

To validate if p16^{INK4a} reduction is epigenetically regulated *p16*^{Ink4a} promoter methylation was examined. Only 1 out of 7 tumors displayed a methylation-specific PCR product (Fig.5A). Next, we investigated the transcriptional level by quantifying *p16*^{Ink4a} mRNA by qRT-PCR. No reduction of *p16*^{Ink4a} mRNA was detected in tumors compared to surrounding normal liver tissue of *Apc*^{homo} mice (Fig.5B, right). In contrast, paradoxically, an increase of *p16*^{Ink4a} mRNA level was detected in all tumors lacking *p16*^{Ink4a} promoter methylation (Fig.5B and Supplementary Fig.S5). The p16^{INK4a} reduction seems post-transcriptionally regulated, probably by increased degradation of p16^{INK4a} protein which would explain increased *p16*^{Ink4a} mRNA levels as compensatory mechanism. Recently, p16^{INK4a} degradation was suggested to occur ubiquitin-independently by PSME3 proteasome (31). Hence, we quantified *Psme3* in tumor and liver extracts and found an up-regulation exclusively in tumor tissue (Fig.5C). Tumor T2-2 in which the *p16*^{Ink4a} promoter is methylated shows no up-regulation of *Psme3* but demonstrates alternatives for p16^{INK4a} reduction in certain cases. Accordingly, this tumor was excluded for statistical analysis of *Psme3* mRNA.

Consequences of altered p16^{INK4a} expression

Overexpression of tumor suppressors, e.g. p16^{INK4a}, leads to induction of senescence associated β-galactosidase (SA-β-Gal; GLB1) (32, 33), activation of the facultative stem cell compartment, oval cells, in phases with proliferation demand (33) and polyploidisation of hepatocytes (33). In all stages of life more SA-β-Gal was detected in cryosections of *Apc*^{homo} compared to *Apc*^{hetero} mice (Fig.6B). However, stronger upregulation of SA-β-Gal was found

in livers of Apc^{KO} mice (Fig.6C) and the strongest reactivity was observed in tissue surrounding tumors and precancerous lesions (Fig.6D). Isolated primary hepatocytes of aged mice revealed in FACS analysis an increase of >16N-ploidy in Apc^{homo} and Apc^{KO} mice (Fig.6E), whereas hepatocytes with 4N-ploidy decreased significantly in Apc^{KO} mice and by trend in Apc^{homo} mice. Immunohistological stainings with anti-pan-cytokeratin antibody specific for oval cells (34), show their activation in Apc^{homo} mice starting at age 5 months. In livers of mice older than 10 months both around macroscopically identifiable tumors and areas of cancer-prestages a border of oval cells was visible (Fig.6J,K, arrows). Hence the question arose what trigger, preferably produced by tumors, could activate oval cell compartment in Apc^{homo} mice.

Recently, Indian hedgehog (IHH) was confirmed as an activator of hepatic stem cells produced by dying hepatocytes (35). We found *Ihh* up-regulated both in cultured hepatocytes after *Apc* siRNA treatment (Fig.6F) and in Apc^{KO} mice (Fig.6F) thus confirming *Ihh* increase in livers of *AhCre-*Apc^{KO} mice (36). These data combined with a trend of *Ihh* reduction in hepatocytes of $Ctnnb1^{KO}$ mice confirm *Ihh* as direct target of β-catenin (37). The up-regulation of *Ihh* mRNA level in tumors (Fig.6F) supports a role as death signal of hepatocytes, and cell damage should be expected.

Evidence of hepatocyte damage

Necrotic cell death occurs in Apc^{KO} mice of every age but also in old Apc^{homo} mice with tumors and prestages (Fig.7A,B). Additionally apoptotic death, featured by numerous Councilman bodies (Fig.7C), seems to play a role in hepatocyte loss of Apc^{homo} mice, at least in aged mice, even though caspase-3 detection failed in all liver slides (not shown). As elevated liver enzymes in serum clearly indicate necrotic loss of hepatocytes, we measured characteristic liver parameters in serum of Apc^{homo}, Apc^{hetero} and Apc^{KO} mice. Although a slight, non-significant raise of ALAT and GLDH activities was detected age-dependently in Apc^{homo} up to the age of 12 months (Fig.7D,F), a significant difference of these enzyme

activities as shown for old mice (Fig.7B,D) between *Apc*^{homo} and *Apc*^{hetero} mice (controls) could be measured at all these ages (not shown). In contrast, serum levels of tumor harbouring mice and *Apc*^{KO} mice were increased up to 10fold compared to age related *Apc*^{homo} mice (Fig.7A-D).

Additionally DNA damage was observed by anti-γ-H2AX staining in all tumors and their prestages (Fig.7K). Moreover, large quantities of γ-H2AX positive nuclei were detected in *Apc*^{KO} mice (Fig.7J).

Discussion

Reduced APC expression leads to permanent activation of β-catenin and consequently, to upregulation of Wnt/β-catenin target genes and a pericentral expression program (12, 28, 38). Conversely, *Hras* mutations cause a periportal expression program (28). Unexpectedly, livers of *Apc*^{homo} mice, providing a model of half-maximal β-catenin activation, develop phenotypically different tumors. Some of them are distinguished by the expression of the Wnt-target gene *Glul* and others by detection of E-cadherin, which is actually downregulated by sufficient β-catenin activation and belongs to the periportal expression program. Other Wnt-target genes, i.e. *Axin2*, are reduced or unchanged in such tumors ((12), present study). Likewise, the periportally expressed protein CPS is heterogeneously expressed.

The tumor suppressor *p16*^{INK4a}, recently identified as a β-catenin target gene (27), was completely lost at protein level in all tumors and precancerous lesions investigated here and results in bypassing senescence as recently also found in human HCC and hepatoblastoma (39, 40).

Our data suggest the epigenetic silencing of *p16*^{Ink4a} in selected liver cells is a common factor for development of liver tumors. Firstly, APC reduction leads to overexpression of p16^{INK4a} in the unaffected healthy liver of *Apc*^{homo} mice and in hepatocytes of *Apc*^{KO} mice with highly

activated β-catenin signaling. Subsequently, elevated $p16^{INK4a}$ induces senescence and protects from tumorigenesis as recently shown by others for pre-malignant hepatocytes in mice (41). Necessarily, increased ALAT and GLDH levels in Apc^{homo} mice indicate loss of pericentrally programmed hepatocytes, which culminates in permanent proliferative stress of residual hepatocytes, being still senescent by $p16^{INK4a}$ overexpression. Thereby no fully replicative senescence seems to occur, because growth and physiological function of liver of Apc^{homo} mice are not limited up to a critical age of about 10 months when tumors develop. Because the replicative capacity of hepatocytes is impaired by $p16^{INK4a}$ overexpression, a physiologically required hepatocyte replacement generates a selective pressure, both forcing the initiation of $p16^{Ink4a}$ silencing in selected populations of hepatocytes and promoting subsequent proliferation of clusters of $p16^{INK4a}$ negative hepatocytes. We hypothesize this sequence of events because no single $p16^{INK4a}$ negative hepatocyte was detected in younger animals before precancerous lesions occur and hyperproliferation does also not occur by moderate/half-maximal activated hepatocytes.

It seems irrelevant which metabolic program (pericentral/periportal phenotype) is followed by $p16^{Ink4a}$ silenced cells. The most relevant process responsible for silencing of $p16^{Ink4a}$ function is the specific $p16^{INK4a}$ removal, most likely by PSME3 mediated proteasomal digestion.

The $p16^{INK4a}$ overexpression induced by diminished APC levels supports faster ageing and death of hepatocytes, which therefore contain a diminished proliferative capacity. A similar explanation can be supposed to pericentral hepatocytes, which have a continuous β-catenin signaling (42), and might also be relevant in liver parenchyma of FAP patients as shown here by GLUL expression. $P16^{INK4a}$ up-regulation as a consequence of *APC*-repressing mutations also occurs in hepatocytes of FAP patients and likely protects from liver cancer in early stages of life in the majority of cases. The higher incidence of hepatoblastoma in children with FAP (43) and the frequent occurrence of $p16^{INK4a}$ loss in hepatoblastoma (40) underscores the significance of the tumor supressor $p16^{INK4a}$ in β–catenin activated liver parenchyma.

The escalation of ALAT and GLDH concentrations in Apc^{KO} mice indicates a massive decay of hepatocytes probably causing sudden death of Apc^{KO} mice 10 to 14 days after conditional knockout. The strong γ-H2AX staining in Apc^{KO} mice verifying the replicative stress in Apc^{KO} hepatocytes supports this suggestion.

The IHH signal delivered by dying hepatocytes is obviously not sufficient to activate an adequate number of oval cells to replace lost cells. This also applies to tumors whose elevated *Ihh* levels might follow, additionally to activation by β-catenin, damage induced signals, similarly as reported on radiated hepatocytes (44). Even if sufficient oval cells were activated, their subsequent differentiation into hepatocytes would ultimately end in their decline.

Summarizing, our data suggest the epigenetic silencing of $p16^{Ink4a}$ in selected liver cells bypassing senescence is a common principle for the development of tumors in mouse liver with β-catenin involvement independent of the initial stimulus.

Acknowledgements

We acknowledge the technical assistance of Doris Mahn, Frank Struck, Elisabeth Specht and Helga Stache. We thank Dr. Sabine Colnot (Departement Genetique Developpement et Pathologie Moleculaire, Institut Cochin-INSERM CNRS, University of Paris) for the gift of paraffin slides. Special thanks go to Dr. Helen Scott (University of Bristol, UK) for critically reviewing the manuscript.

References

1 Whittaker,S., Marais,R. and Zhu,A.X. The role of signaling pathways in the development and treatment of hepatocellular carcinoma, Oncogene, *29:* 4989-5005, 2010.

2 Taniguchi,K., Roberts,L.R., Aderca,I.N., Dong,X., Qian,C., Murphy,L.M., Nagorney,D.M., Burgart,L.J., Roche,P.C., Smith,D.I., Ross,J.A. and Liu,W. Mutational spectrum of beta-catenin, AXIN1, and AXIN2 in hepatocellular carcinomas and hepatoblastomas, Oncogene, *21:* 4863-4871, 2002.

3 Lee,J.M., Yang,J., Newell,P., Singh,S., Parwani,A., Friedman,S.L., Nejak-Bowen,K.N. and Monga,S.P. beta-Catenin signaling in hepatocellular cancer: Implications in inflammation, fibrosis, and proliferation, Cancer Lett., *343:* 90-97, 2014.

4 Ihara,A., Koizumi,H., Hashizume,R. and Uchikoshi,T. Expression of epithelial cadherin and alpha- and beta-catenins in nontumoral livers and hepatocellular carcinomas, Hepatology., *23:* 1441-1447, 1996.

5 Zucman-Rossi,J., Benhamouche,S., Godard,C., Boyault,S., Grimber,G., Balabaud,C., Cunha,A.S., Bioulac-Sage,P. and Perret,C. Differential effects of inactivated Axin1 and activated beta-catenin mutations in human hepatocellular carcinomas, Oncogene., *26:* 774-780, 2007.

6 de La,C.A., Romagnolo,B., Billuart,P., Renard,C.A., Buendia,M.A., Soubrane,O., Fabre,M., Chelly,J., Beldjord,C., Kahn,A. and Perret,C. Somatic mutations of the beta-catenin gene are frequent in mouse and human hepatocellular carcinomas, Proc Natl Acad Sci U S A., *95:* 8847-8851, 1998.

7 Satoh,S., Daigo,Y., Furukawa,Y., Kato,T., Miwa,N., Nishiwaki,T., Kawasoe,T., Ishiguro,H., Fujita,M., Tokino,T., Sasaki,Y., Imaoka,S., Murata,M., Shimano,T., Yamaoka,Y. and Nakamura,Y. AXIN1 mutations in hepatocellular carcinomas, and growth suppression in cancer cells by virus-mediated transfer of AXIN1, Nat Genet., *24:* 245-250, 2000.

8 Lustig,B., Jerchow,B., Sachs,M., Weiler,S., Pietsch,T., Karsten,U., van de,W.M., Clevers,H., Schlag,P.M., Birchmeier,W. and Behrens,J. Negative feedback loop of Wnt signaling through upregulation of conductin/axin2 in colorectal and liver tumors, Mol Cell Biol., *22:* 1184-1193, 2002.

9 Ishizaki,Y., Ikeda,S., Fujimori,M., Shimizu,Y., Kurihara,T., Itamoto,T., Kikuchi,A., Okajima,M. and Asahara,T. Immunohistochemical analysis and mutational analyses of beta-catenin, Axin family and APC genes in hepatocellular carcinomas, Int J Oncol., *24:* 1077-1083, 2004.

10 Csepregi,A., Rocken,C., Hoffmann,J., Gu,P., Saliger,S., Muller,O., Schneider-Stock,R., Kutzner,N., Roessner,A., Malfertheiner,P. and Ebert,M.P. APC promoter methylation and protein expression in hepatocellular carcinoma, J Cancer Res Clin.Oncol., *134:* 579-589, 2008.

11 Kinzler,K.W. and Vogelstein,B. Lessons from hereditary colorectal cancer, Cell., *87:* 159-170, 1996.

12 Buchert,M., Athineos,D., Abud,H.E., Burke,Z.D., Faux,M.C., Samuel,M.S., Jarnicki,A.G., Winbanks,C.E., Newton,I.P., Meniel,V.S., Suzuki,H., Stacker,S.A., Nathke,I.S., Tosh,D., Huelsken,J., Clarke,A.R., Heath,J.K., Sansom,O.J. and Ernst,M. Genetic dissection of differential signaling threshold requirements for the Wnt/beta-catenin pathway in vivo, PLoS.Genet., *6:* e1000816, 2010.

13 Shibata,H., Toyama,K., Shioya,H., Ito,M., Hirota,M., Hasegawa,S., Matsumoto,H., Takano,H., Akiyama,T., Toyoshima,K., Kanamaru,R., Kanegae,Y., Saito,I., Nakamura,Y., Shiba,K. and Noda,T. Rapid colorectal adenoma formation initiated by conditional targeting of the Apc gene, Science., *278:* 120-123, 1997.

14 Jho,E.H., Zhang,T., Domon,C., Joo,C.K., Freund,J.N. and Costantini,F. Wnt/beta-catenin/Tcf signaling induces the transcription of Axin2, a negative regulator of the signaling pathway, Mol Cell Biol., *22:* 1172-1183, 2002.

15 Serrano,M., Hannon,G.J. and Beach,D. A new regulatory motif in cell-cycle control causing specific inhibition of cyclin D/CDK4, Nature, *366:* 704-707, 1993.

16 Brault,V., Moore,R., Kutsch,S., Ishibashi,M., Rowitch,D.H., McMahon,A.P., Sommer,L., Boussadia,O. and Kemler,R. Inactivation of the beta-catenin gene by Wnt1-Cre-mediated deletion results in dramatic brain malformation and failure of craniofacial development, Development., *128:* 1253-1264, 2001.

17 Schonig,K., Schwenk,F., Rajewsky,K. and Bujard,H. Stringent doxycycline dependent control of CRE recombinase in vivo, Nucleic Acids Res., *30:* e134, 2002.

18 Kistner,A., Gossen,M., Zimmermann,F., Jerecic,J., Ullmer,C., Lubbert,H. and Bujard,H. Doxycycline-mediated quantitative and tissue-specific control of gene expression in transgenic mice, Proc.Natl.Acad.Sci.U.S.A, *93:* 10933-10938, 1996.

19 Ueberham,E., Aigner,T., Ueberham,U. and Gebhardt,R. E-cadherin as a reliable cell surface marker for the identification of liver specific stem cells, J.Mol.Histol., *38:* 359-368, 2007.

20 Ueberham,E., Bottger,J., Ueberham,U., Grosche,J. and Gebhardt,R. Response of sinusoidal mouse liver cells to choline-deficient ethionine-supplemented diet, Comp Hepatol., *9:* 8, 2010.

21 Seglen,P.O. Preparation of isolated rat liver cells, Methods Cell Biol., *13:* 29-83, 1976.

22 Quistorff,B., Grunnet,N. and Cornell,N.W. Digitonin perfusion of rat liver. A new approach in the study of intra-acinar and intracellular compartmentation in the liver, Biochem.J., *226:* 289-297, 1985.

23 Gebhardt,R. Isolation of periportal and pericentral hepatocytes, Methods Mol Biol., *107:319-28.:* 319-328, 1998.

24 Lindner,I., Hemdan,N.Y., Buchold,M., Huse,K., Bigl,M., Oerlecke,I., Ricken,A., Gaunitz,F., Sack,U., Naumann,A., Hollborn,M., Thal,D., Gebhardt,R. and Birkenmeier,G. Alpha2-macroglobulin inhibits the malignant properties of astrocytoma cells by impeding beta-catenin signaling, Cancer Res., *70:* 277-287, 2010.

25 Sharpless,N.E., Bardeesy,N., Lee,K.H., Carrasco,D., Castrillon,D.H., Aguirre,A.J., Wu,E.A., Horner,J.W. and DePinho,R.A. Loss of p16Ink4a with retention of p19Arf predisposes mice to tumorigenesis, Nature, *413:* 86-91, 2001.

26 Torre,C., Perret,C. and Colnot,S. Transcription dynamics in a physiological process: beta-catenin signaling directs liver metabolic zonation, Int.J.Biochem.Cell Biol., *43:* 271-278, 2011.

27 Wassermann,S., Scheel,S.K., Hiendlmeyer,E., Palmqvist,R., Horst,D., Hlubek,F., Haynl,A., Kriegl,L., Reu,S., Merkel,S., Brabletz,T., Kirchner,T. and Jung,A. p16INK4a is a beta-catenin target gene and indicates low survival in human colorectal tumors, Gastroenterology, *136:* 196-205, 2009.

28 Hailfinger,S., Jaworski,M., Braeuning,A., Buchmann,A. and Schwarz,M. Zonal gene expression in murine liver: lessons from tumors, Hepatology., *43:* 407-414, 2006.

29 Colnot,S., Decaens,T., Niwa-Kawakita,M., Godard,C., Hamard,G., Kahn,A., Giovannini,M. and Perret,C. Liver-targeted disruption of Apc in mice activates beta-catenin signaling and leads to hepatocellular carcinomas, Proc Natl Acad Sci U S A., *101:* 17216-17221, 2004.

30 Cole,A.M., Ridgway,R.A., Derkits,S.E., Parry,L., Barker,N., Clevers,H., Clarke,A.R. and Sansom,O.J. p21 loss blocks senescence following Apc loss and provokes tumourigenesis in the renal but not the intestinal epithelium, EMBO Mol Med., *2:* 472-486, 2010.

31 Chen,X., Barton,L.F., Chi,Y., Clurman,B.E. and Roberts,J.M. Ubiquitin-independent degradation of cell-cycle inhibitors by the REGgamma proteasome, Mol.Cell, *26:* 843-852, 2007.

32 Sigal,S.H., Rajvanshi,P., Gorla,G.R., Sokhi,R.P., Saxena,R., Gebhard,D.R., Jr., Reid,L.M. and Gupta,S. Partial hepatectomy-induced polyploidy attenuates hepatocyte replication and activates cell aging events, Am.J.Physiol, *276:* G1260-G1272, 1999.

33 Ueberham,E., Lindner,R., Kamprad,M., Hiemann,R., Hilger,N., Woithe,B., Mahn,D., Cross,M., Sack,U., Gebhardt,R., Arendt,T. and Ueberham,U. Oval cell proliferation in p16(INK4a) expressing mouse liver is triggered by chronic growth stimuli, J.Cell Mol.Med., *12:* 622-638, 2008.

34 Kofman,A.V., Morgan,G., Kirschenbaum,A., Osbeck,J., Hussain,M., Swenson,S. and Theise,N.D. Dose- and time-dependent oval cell reaction in acetaminophen-induced murine liver injury, Hepatology, *41:* 1252-1261, 2005.

35 Omenetti,A., Choi,S., Michelotti,G. and Diehl,A.M. Hedgehog signaling in the liver, J.Hepatol., *54:* 366-373, 2011.

36 Reed,K.R., Athineos,D., Meniel,V.S., Wilkins,J.A., Ridgway,R.A., Burke,Z.D., Muncan,V., Clarke,A.R. and Sansom,O.J. B-catenin deficiency, but not Myc deletion, suppresses the immediate phenotypes of APC loss in the liver, Proc Natl Acad Sci U S A., *105:* 18919-18923, 2008.

37 Burke,Z.D., Reed,K.R., Phesse,T.J., Sansom,O.J., Clarke,A.R. and Tosh,D. Liver zonation occurs through a beta-catenin-dependent, c-Myc-independent mechanism, Gastroenterology, *136:* 2316-2324, 2009.

38 Benhamouche,S., Decaens,T., Godard,C., Chambrey,R., Rickman,D.S., Moinard,C., Vasseur-Cognet,M., Kuo,C.J., Kahn,A., Perret,C. and Colnot,S. Apc tumor suppressor gene is the "zonation-keeper" of mouse liver, Dev.Cell., *10:* 759-770, 2006.

39 Lu,W.J., Chua,M.S. and So,S.K. Suppressing N-Myc downstream regulated gene 1 reactivates senescence signaling and inhibits tumor growth in hepatocellular carcinoma, Carcinogenesis., *35:* 915-922, 2014.

40 Shim,Y.H., Park,H.J., Choi,M.S., Kim,J.S., Kim,H., Kim,J.J., Jang,J.J. and Yu,E. Hypermethylation of the p16 gene and lack of p16 expression in hepatoblastoma, Mod.Pathol., *16:* 430-436, 2003.

41 Kang,T.W., Yevsa,T., Woller,N., Hoenicke,L., Wuestefeld,T., Dauch,D., Hohmeyer,A., Gereke,M., Rudalska,R., Potapova,A., Iken,M., Vucur,M., Weiss,S., Heikenwalder,M., Khan,S., Gil,J., Bruder,D., Manns,M., Schirmacher,P., Tacke,F., Ott,M., Luedde,T., Longerich,T., Kubicka,S. and Zender,L. Senescence surveillance of pre-malignant hepatocytes limits liver cancer development, Nature., *479:* 547-551, 2011.

42 Moriyama,A., Kii,I., Sunabori,T., Kurihara,S., Takayama,I., Shimazaki,M., Tanabe,H., Oginuma,M., Fukayama,M., Matsuzaki,Y., Saga,Y. and Kudo,A. GFP transgenic mice reveal active canonical Wnt signal in neonatal brain and in adult liver and spleen, Genesis., *45:* 90-100, 2007.

43 Gupta,A., Sheridan,R.M., Towbin,A., Geller,J.I., Tiao,G. and Bove,K.E. Multifocal hepatic neoplasia in 3 children with APC gene mutation, Am.J Surg.Pathol., *37:* 1058-1066, 2013.

44 Wang,S., Lee,Y., Kim,J., Hyun,J., Lee,K., Kim,Y. and Jung,Y. Potential role of Hedgehog pathway in liver response to radiation, PLoS.ONE., *8:* e74141, 2013.

Figure legends

Figure 1

Activation of canonical β-catenin signaling in liver of *Apc*^{homo} mice

A-D) Immunohistochemistry of mouse liver sections with anti-β-catenin antibody.

Though some hepatocytes with nuclear β-catenin are detected in liver parenchyma of young *Apc*^{homo} mice (**A,A'**), the staining pattern is mainly comparable to normal liver (not shown) with β-catenin detection at hepatocyte membrane. A pronounced nuclear staining of β-catenin is induced in *Apc*^{KO} mice (**B,B'**). Aged *Apc*^{homo} mice have clusters of hepatocytes with nuclear β-catenin staining (**C and** right edge in **C**') and have both tumor prestages and tumors without nuclear β-catenin (**C'**) and with nuclear β-catenin (**D**,**D'**). **C'** and **D'** represent larger magnifications of framed areas in **C** and **D**. Scale bar, A,B,C,D, 1200 µm; A´,B´,C´,D´, 40 µm.

E-F) Quantification of *Axin2* mRNA (**E**) in livers of different transgenic mice and tumor tissue of aged *Apc*^{homo} mice by qRT-PCR; *, $p<0.05$, $n>4$, t-test, and (**F**) in single individual tumors of aged *Apc*^{homo} mice. T represents individual tumors, i.e. T2-1 indicates tumor 2 in mouse 1.

G-J) Differential activation of β-catenin. (**G**) Activity of the *Top-Gau* luciferase reporter (containing two sets of three copies of TCF binding site and a soluble *Gaussia princeps* luciferase) displays differential β-catenin activation *in vitro* in cultured primary hepatocytes (hep) of *Apc*^{homo}, *Apc*^{KO} and *Ctnnb1*^{KO} mice related to control mice 48 hours post transfection, $p<0.05$, $n=4$ (For each group hepatocytes of four different animals were used), Mann-Whitney test.

Demonstration of Wnt/β-catenin signaling in liver sections of *Apc*^{hetero}/*Conductin*$^{+/lacZ}$ mice (**H**) and *Apc*^{homo}/*Conductin*$^{+/lacZ}$ mice (**J**) by enzyme-immunohistochemistry of β-

galactosidase using X-Gal as substrate displays a distinct turquoise reaction product. Scale bar, 50 µm.

Figure 2

Immunohistochemistry of marker proteins zonally expressed in mouse and human liver

(**A**) Spreading of pericentral (GLUL, CYP2E1) and periportal (CPS, E-cadherin) specific proteins over the liver lobe in *Apc*^{homo} mice at different ages

Using rabbit anti-CPS I, mouse anti-GLUL, mouse anti-E-cadherin and rabbit anti-CYP2E1 antibodies the distribution of indicated pericentral and periportal proteins is immunohistochemically demonstrated (brown, DAB). Liver sections of 8 week old *Apc*^{hetero} mice, used as controls, show the localisation of the proteins in normal mouse liver, because no differences were detected between C57BL/6 and *Apc*^{hetero} mouse liver at different ages (not shown). Central veins were indicated by cv, portal tracts by pv. Bar represents 100 µm.

(**B**) Distribution of the pericentral marker enzyme GLUL in human liver sections

Immunohistochemistry with anti-GLUL antibody (brown, DAB) was performed on representative normal human liver sections and liver sections of FAP patients.

Figure 3

Expression of typical pericentral and periportal proteins in tumors and precancerous lesions in aged *Apc*^{homo} mice (>10 months)

Serial liver sections of different tumor harbouring mice were immunohistochemically stained using antibodies against GLUL and CYP2E1, which represent pericentrally expressed proteins in normal liver and CPS and E-cadherin, which exhibit periportally expressed proteins in normal mouse liver. From left to right the following HCC phenotypes are shown: GLUL positive, GLUL negative, mixed phenotype and tumor prestages. Scale bar, 100 µm.

Figure 4

P16^{INK4a} expression in HCCs of mouse liver

(**A**) Serial liver sections of tumor-containing *Apc^{homo}* (13) mouse, (**B**) *Apc$^{flox/flox}$* mouse *in vivo* transfected with adenoviral *Cre* (29) and (**C**) mice with chemically induced HCCs (28) were incubated either with anti-GLUL and anti-p16^{INK4a} or anti-E-cadherin and anti-p16^{INK4a} antibodies. Positively labelled signals are brown (DAB). Chemically induced tumors had been generated by a N-nitrosodiethylamine/ phenobarbital initation protocol, with a single i.p. dosage of the nitrosamine (90µg/g body weight) at 6 weeks of age followed by phenobarbital-containing diet (0.05%) for 6 months. Scale bar, 100 µm.

Figure 5

Cause of p16^{INK4a} reduction in mouse liver tumors

A) Methylation-specific PCR proved epigenetic silencing of *p16^{Ink4a}* promoter.

DNA of seven different tumors was examined by PCR using primers specific for methylated (m) and unmethylated (um) *p16^{Ink4a}*-promoter. As controls a methylated DNA (positive-m; Zymed research) and DNA of tumor T1-1 surrounding liver tissue of an *Apc^{homo}* mouse (homo-m, homo-um) were used. Abbreviations: see legend of Fig.1B.

B) Quantification of *p16^{Ink4a}* expression in isolated hepatocytes and liver tissue extracts by qRT-PCR.

Mean relative mRNA content of pericentral hepatocytes of *Apc^{homo}* (pc-*Apc^{homo}*, n=6), hepatocytes of *Apc^{KO}* (hep-*Apc^{KO}*, n=3) and *Apc^{homo}* (hep-*Apc^{homo}*, n=3) mice, and *Apc^{homo}* liver tissue (tissue-*Apc^{homo}*, n=6) and tumor tissue of *Apc^{homo}* mice (n=7) was compared to the mean value provided by hepatocytes of 5 control animals which were used as reference. The highest, but equal, *p16^{Ink4a}* expression was measured in tumor and surrounding liver tissue of *Apc^{homo}* mice, *, $p<0.05$, Mann-Whitney test. Tissue of tumor 2-2 possesses decreased p16^{INK4a} mRNA compared to control (see Supplementary Fig.S5).

C) QRT-PCR of *Psme3* mRNA in liver extracts of indicated mice and tumors of Apc^{homo} mice and in separately isolated individual tumors (see also legend Fig.1), *, $p<0.05$, Mann-Whitney test.

Figure 6

Signals of senescence in Apc^{homo} mice

(A-D) Enzyme-histochemistry of SA-β-Gal in liver cryosections of control (Apc^{hetero}) **(A)**, Apc^{homo} **(B)**, Apc^{KO} **(C)** and tumor-containing aged Apc^{homo} mice **(D)**. The turquoise color is the reaction product of SA-β-Gal activity with substrate X-Gal at pH 6.0. Dotted line in **D** marks the border between tumor, visible on the upper right edge, and non-tumor. Scale bar, 50 μm.

Altered hepatocyte ploidy and DNA content respectively was determined by flow cytometry analysis using propidium iodide staining **(E)**. Apc^{hetero} mice possess more hepatocytes with 4N DNA content than Apc^{KO} mice. Hepatocytes with higher ploidy, >16N, were over-represented in Apc^{homo} and Apc^{KO} mice compared to controls (Apc^{hetero}), *, $p<0.05$, t-test. **(F)** *Ihh* mRNA was measured by qRT-PCR in isolated hepatocytes and in extracts of whole liver. Data represent fold change in positive direction for induction and in negative direction for repression of *Ihh* mRNA. The ratio of *Ihh* mRNA in Apc^{hetero} mouse liver normalised to *cyclophilin* mRNA represents the benchmark, *, $p<0.05$, Mann-Whitney test.

Abbreviations: hep, total hepatocytes; pc, pericentral hepatocytes; tissue, liver tissue; hep-wt-*Apc*-si, C57BL/6-hepatocytes transfected with *Apc* siRNA.

(G-K) Depiction of oval cells by cytokeratin immunoreactivity.

Liver sections of Apc^{hetero} **(G)** and Apc^{homo} **(H-K)** mice, each 10 months old, were immunohistochemically stained with an anti-cytokeratin antibody combined to a biotinylated secondary antibody (brown; DAB) Arrows indicate the remarkable border of oval cells surrounding tumor prestages. Scale bar, 50 μm.

Figure 7

Evidence of hepatocyte damage in Apc^{homo} and Apc^{KO} mice

(A-C) Hematoxylin/Eosin staining of liver sections of Apc^{KO} (**A**) and old Apc^{homo} mice **(B,D)** demonstrating the ruin of hepatocytes by necrosis (black arrows in **A** and **B**) and by apoptosis (black arrows in **C**).

(D-G) Serum enzyme activity of GLDH **(D)** and ALAT **(F)** in Apc^{homo} and Apc^{KO} mice at different ages and compared to activities in control mice (Apc^{hetero}) as indicated **(E,G)**, Mann-Whitney test, *, $p<0.02$.

(E-G) Immunohistochemistry with rabbit anti-γ-H2AX detects DNA damage in (**H**) control (Apc^{hetero}), (**J**) Apc^{KO} and (**K**) Apc^{homo} mice (brown nuclei, DAB). The dashed line in (**G**) marks the border to the tumor (*). Scale bar, 50 μm.

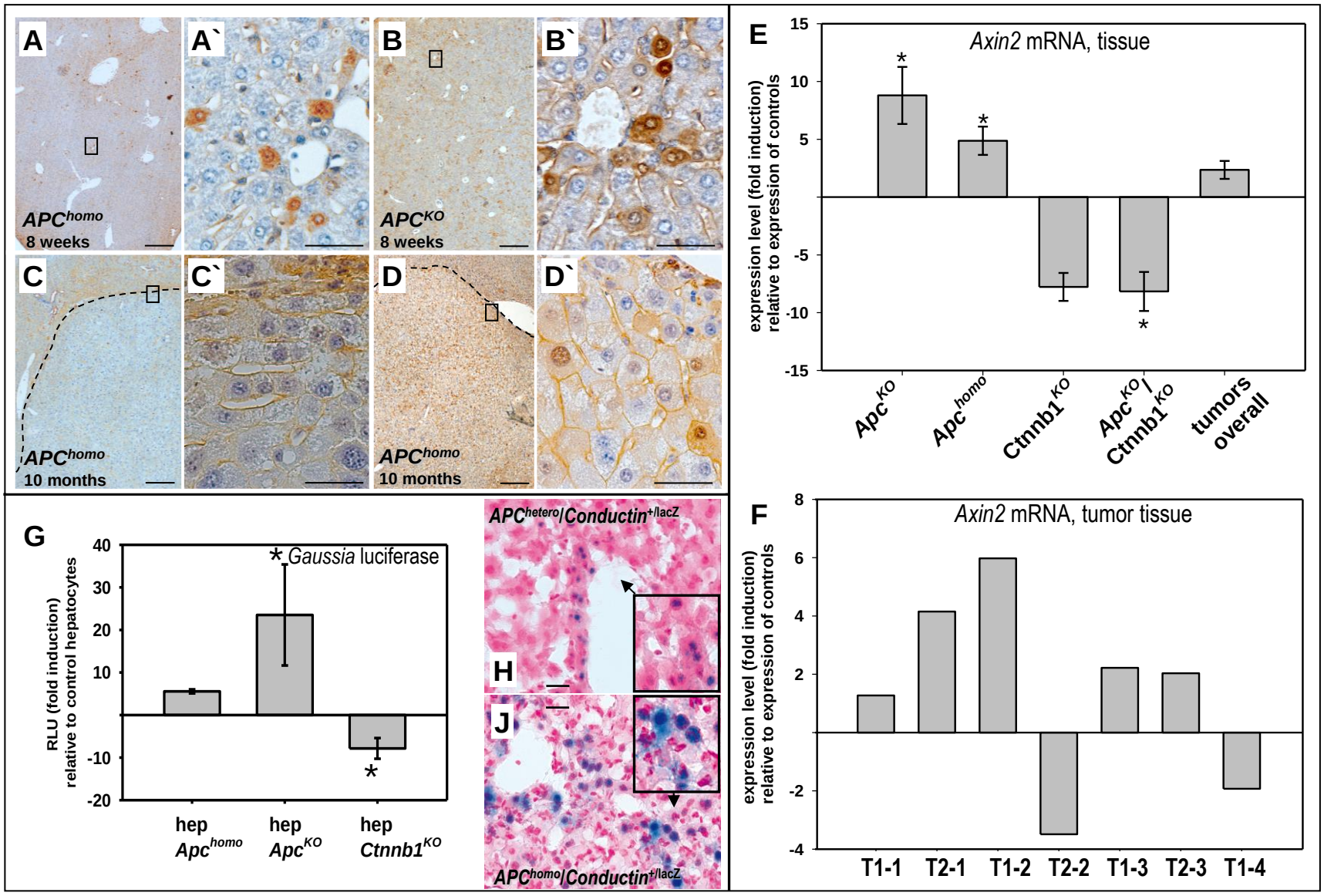
A
A`
B
B`
APC^homo
8 weeks
APC^KO
8 weeks
C
C`
D
D`
APC^homo
10 months
APC^homo
10 months
E
Axin2 mRNA, tissue
expression level (fold induction)
relative to expression of controls
15
10
5
-5
-10
-15
Apc^KO
Apc^homo
Ctnnb1^KO
Apc^KO / Ctnnb1^KO
tumors overall
F
Axin2 mRNA, tumor tissue
expression level (fold induction)
relative to expression of controls
8
6
4
2
-2
-4
T1-1
T2-1
T1-2
T2-2
T1-3
T2-3
T1-4
G
Gaussia luciferase
RLU (fold induction)
relative to control hepatocytes
40
30
20
10
-10
-20
hep Apc^homo
hep Apc^KO
hep Ctnnb1^KO
APC^hetero/Conductin^+/lacZ
H
J
APC^homo/Conductin^+/lacZ

Figure 1

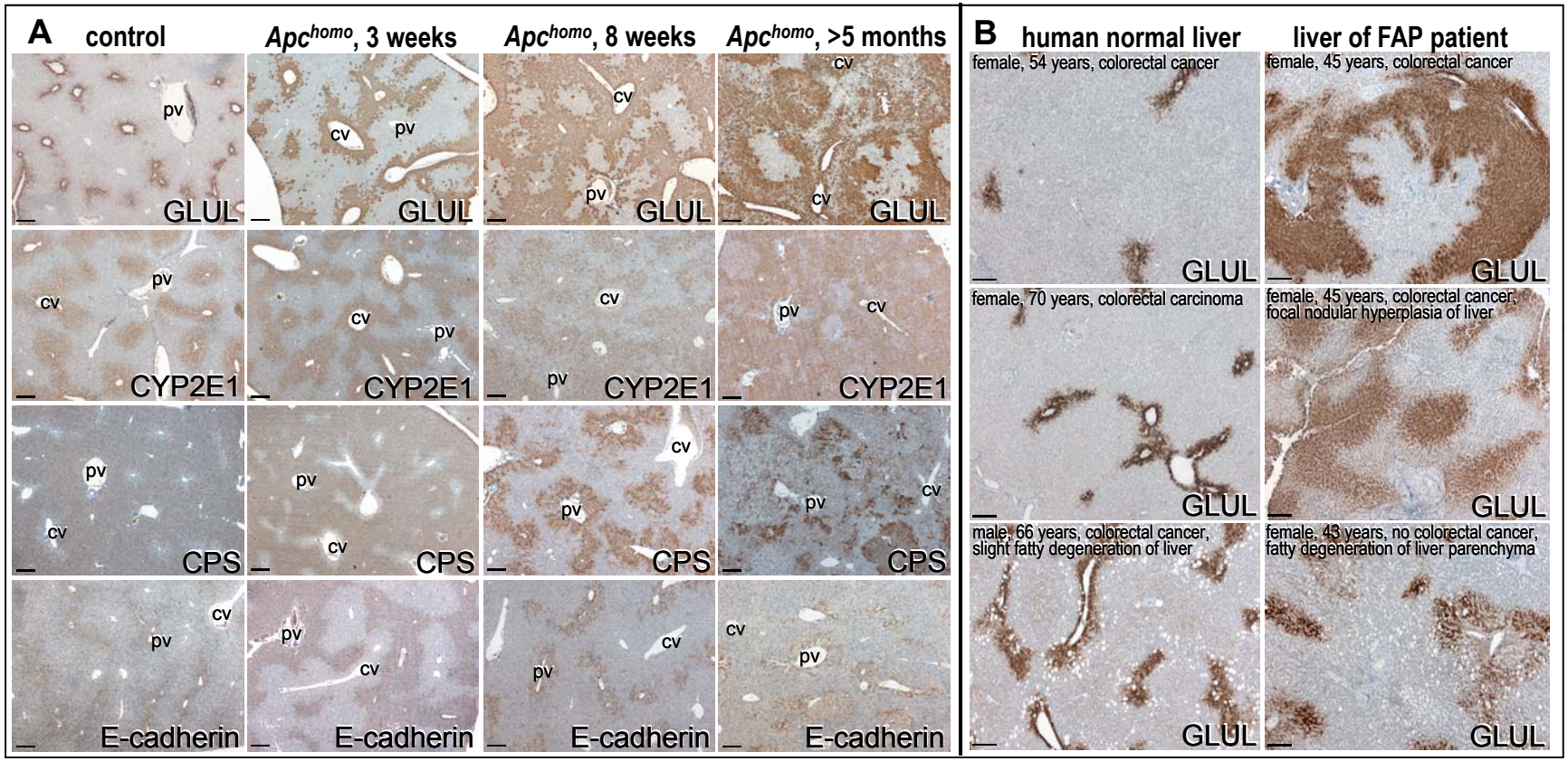
A
control
Apc^homo, 3 weeks
Apc^homo, 8 weeks
Apc^homo, >5 months
GLUL
CYP2E1
CPS
E-cadherin
pv
cv
B
human normal liver
liver of FAP patient
female, 54 years, colorectal cancer
female, 45 years, colorectal cancer
female, 70 years, colorectal carcinoma
female, 45 years, colorectal cancer; focal nodular hyperplasia of liver
male, 66 years, colorectal cancer; slight fatty degeneration of liver
female, 43 years, no colorectal cancer; fatty degeneration of liver parenchyma
GLUL

Figure 2

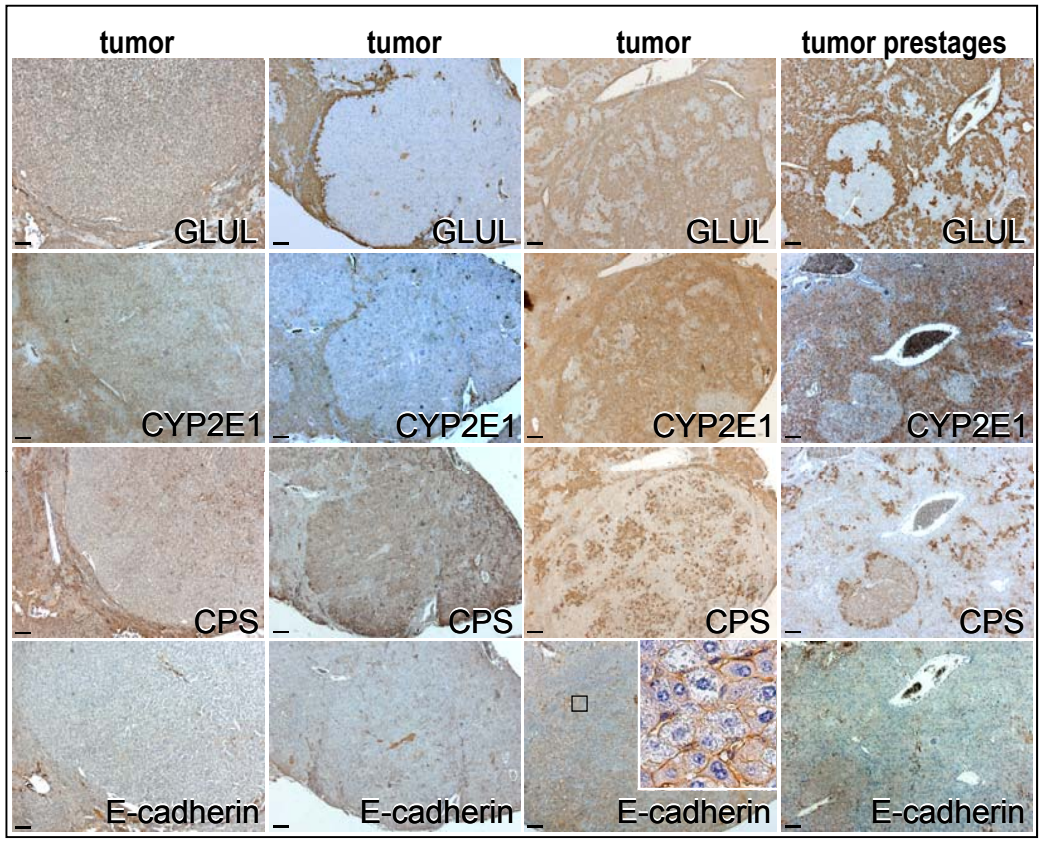
tumor
tumor
tumor
tumor prestages
GLUL
GLUL
GLUL
GLUL
CYP2E1
CYP2E1
CYP2E1
CYP2E1
CPS
CPS
CPS
CPS
E-cadherin
E-cadherin
E-cadherin
E-cadherin

Figure 3

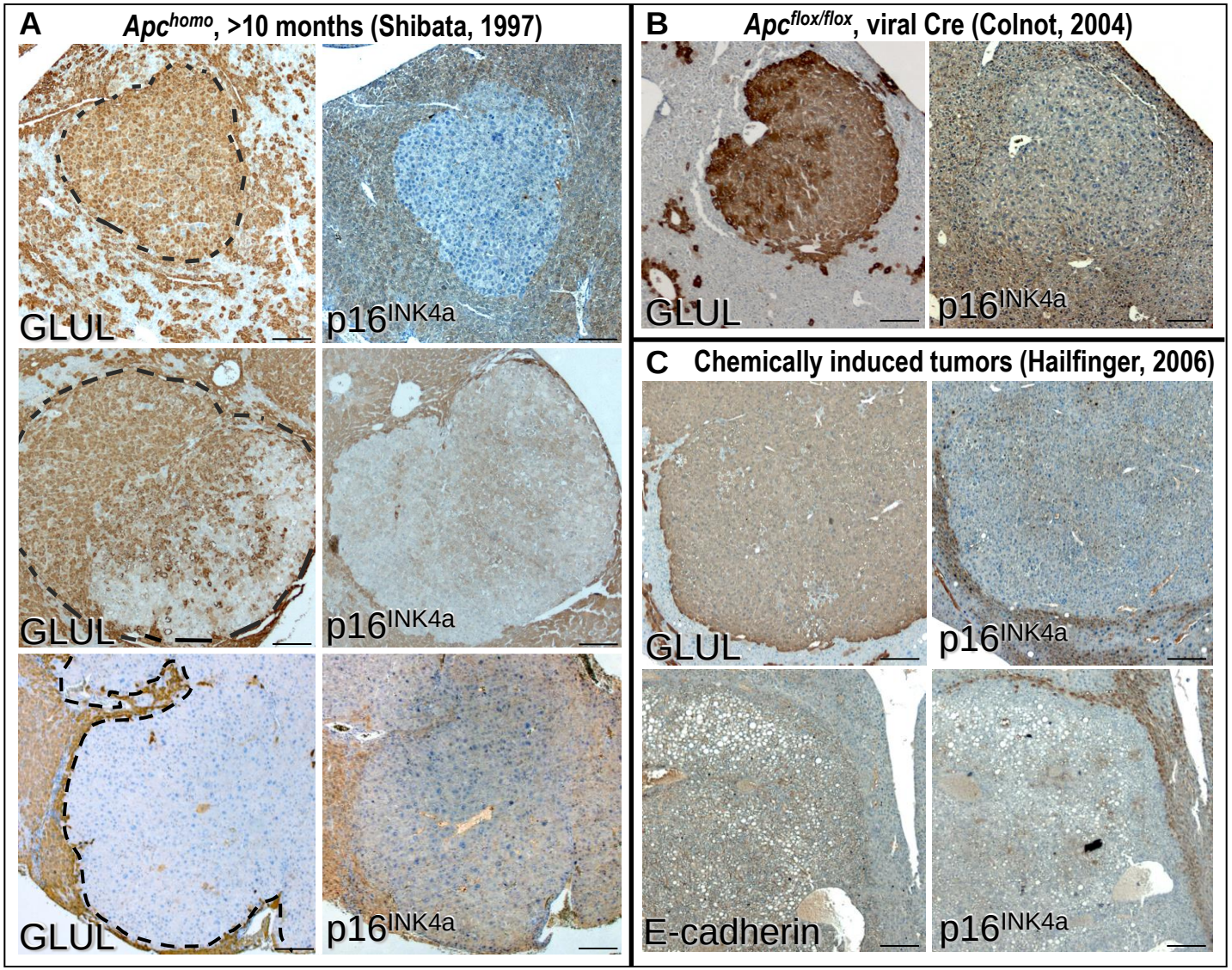
A
Apc^homo, >10 months (Shibata, 1997)
GLUL
p16INK4a
GLUL
p16INK4a
GLUL
p16INK4a
B
Apc^flox/flox, viral Cre (Colnot, 2004)
GLUL
p16INK4a
C
Chemically induced tumors (Hailfinger, 2006)
GLUL
p16INK4a
E-cadherin
p16INK4a

Figure 4

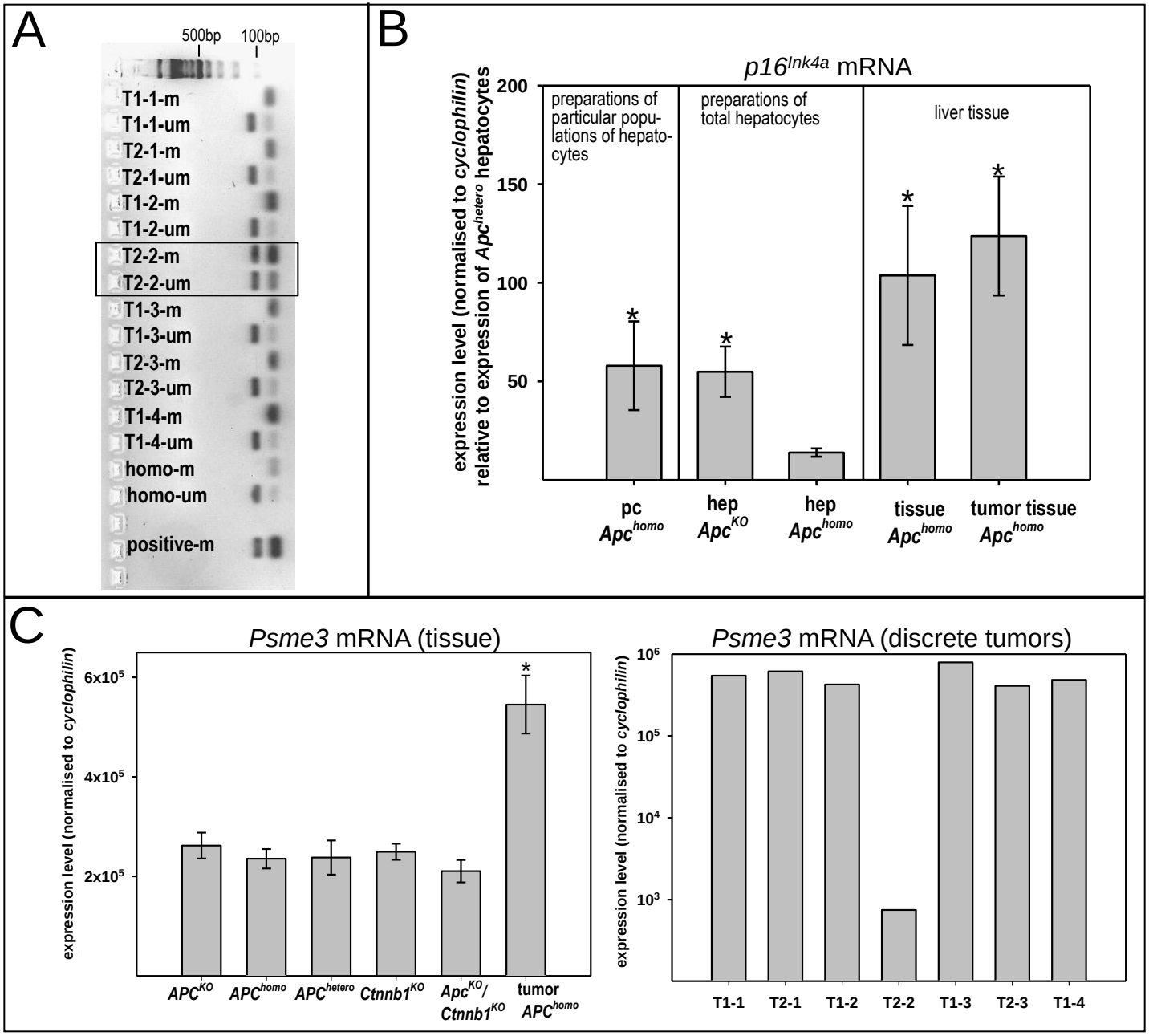
A
500bp
100bp
T1-1-m
T1-1-um
T2-1-m
T2-1-um
T1-2-m
T1-2-um
T2-2-m
T2-2-um
T1-3-m
T1-3-um
T2-3-m
T2-3-um
T1-4-m
T1-4-um
homo-m
homo-um
positive-m
B
p16Ink4a mRNA
expression level (normalised to cyclophilin) relative to expression of Apchetero hepatocytes
200
150
100
50
preparations of particular populations of hepatocytes
preparations of total hepatocytes
liver tissue
pc Apchomo
hep APCKO
hep Apchomo
tissue Apchomo
tumor tissue Apchomo
C
Psme3 mRNA (tissue)
expression level (normalised to cyclophilin)
6x10^5
4x10^5
2x10^5
APCKO
APChomo
APChetero
Ctnnb1KO
ApcKO/ Ctnnb1KO
tumor APChomo
Psme3 mRNA (discrete tumors)
expression level (normalised to cyclophilin)
10^6
10^5
10^4
10^3
T1-1
T2-1
T1-2
T2-2
T1-3
T2-3
T1-4

Figure 5

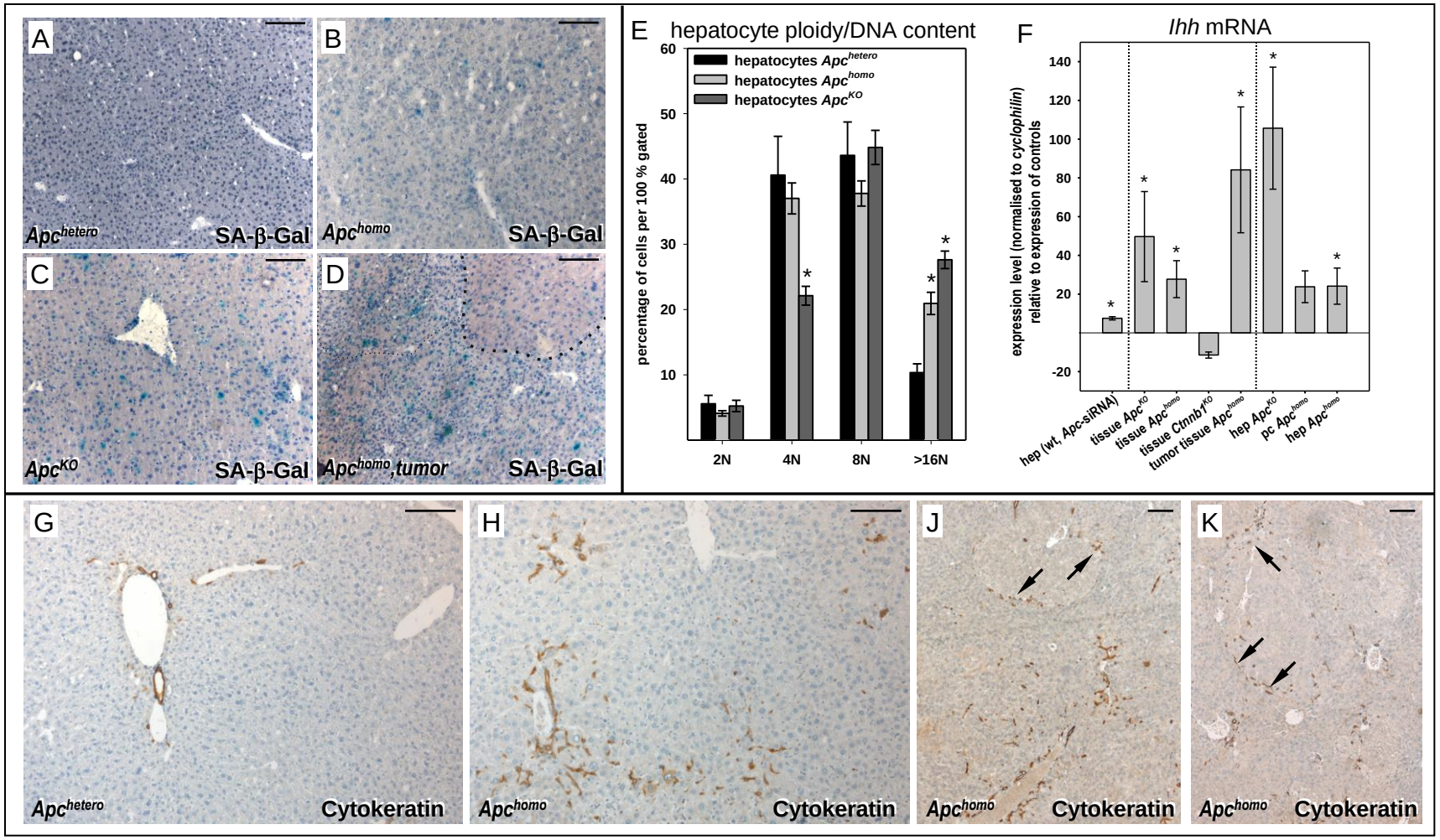
A
Apc^hetero
SA-β-Gal
B
Apc^homo
SA-β-Gal
C
Apc^KO
SA-β-Gal
D
Apc^homo,tumor
SA-β-Gal
E
hepatocyte ploidy/DNA content
hepatocytes Apc^hetero
hepatocytes Apc^homo
hepatocytes Apc^KO
percentage of cells per 100 % gated
60
50
40
30
20
10
2N
4N
8N
>16N
F
Ihh mRNA
expression level (normalised to cyclophilin) relative to expression of controls
140
120
100
80
60
40
20
-20
hep (wt, Apc-siRNA)
tissue Apc^KO
tissue Apc^homo
tissue Ctnnb1^KO
tumor tissue Apc^homo
hep Apc^KO
pc Apc^homo
hep Apc^homo
G
Apc^hetero
Cytokeratin
H
Apc^homo
Cytokeratin
J
Apc^homo
Cytokeratin
K
Apc^homo
Cytokeratin

Figure 6

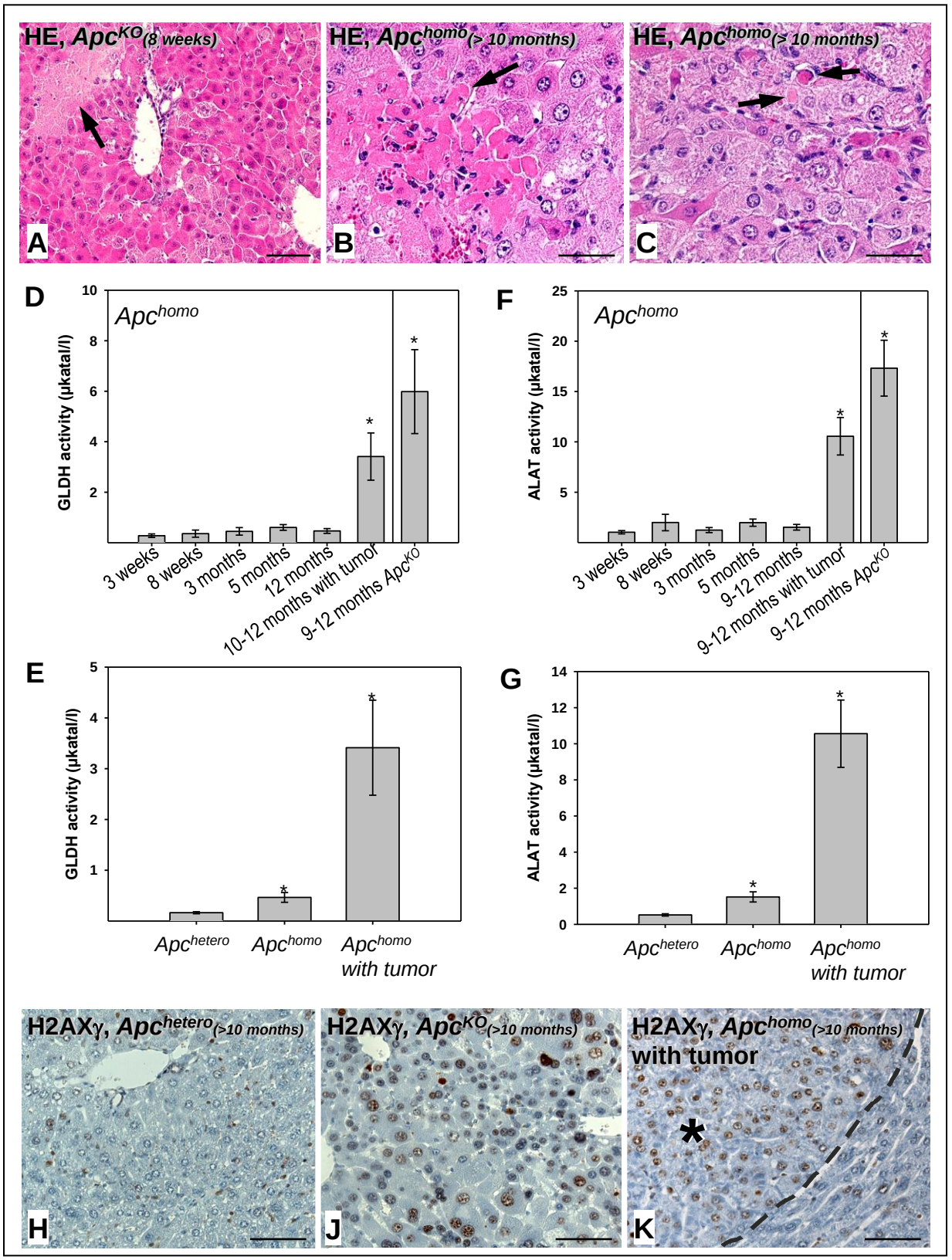
HE, Apc^KO (8 weeks)
HE, Apc^homo (> 10 months)
HE, Apc^homo (> 10 months)
A
B
C
D
Apc^homo
GLDH activity (µkatal/l)
3 weeks
8 weeks
3 months
5 months
12 months
10-12 months with tumor
9-12 months Apc^KO
F
Apc^homo
ALAT activity (µkatal/l)
3 weeks
8 weeks
3 months
5 months
9-12 months
9-12 months with tumor
9-12 months Apc^KO
E
GLDH activity (µkatal/l)
Apc^hetero
Apc^homo
Apc^homo with tumor
G
ALAT activity (µkatal/l)
Apc^hetero
Apc^homo
Apc^homo with tumor
H2AXγ, Apc^hetero (>10 months)
H2AXγ, Apc^KO (>10 months)
H2AXγ, Apc^homo (>10 months) with tumor
H
J
K

Figure 7